

Supporting Information for:

## An Enantiomeric Pair of Alkaline-Earth Metal Based Coordination Polymers Showing Room Temperature Phosphorescence and Circularly Polarized Luminescence

Pedro Leo,<sup>a\*</sup> Gisela Orcajo,<sup>b</sup> Jose A. García,<sup>c</sup> Ana M. Ortuño,<sup>d</sup> Juan M. Cuerva,<sup>d</sup> David Briones,<sup>a</sup> Guillermo Calleja,<sup>b</sup> Antonio Rodríguez-Diéguez,<sup>c</sup> Raul Sanz,<sup>b</sup> Javier Cepeda<sup>f\*</sup> and Fernando Martínez<sup>a</sup>

<sup>a</sup> *Departamento de Tecnología Química y Ambiental, Universidad Rey Juan Carlos, Calle Tulipán s/n, 28933 Móstoles, Spain.* <sup>b</sup> *Departamento de Tecnología Química, Energética y Mecánica, Universidad Rey Juan Carlos, Calle Tulipán s/n, 28933 Móstoles, Spain.* <sup>c</sup> *Departamento de Física Aplicada II, Facultad de Ciencia y Tecnología, University of the Basque Country (UPV/EHU), 48940 Leioa, Spain.* <sup>d</sup> *Departamento de Química Orgánica, UEQ, Facultad de Ciencias, Universidad de Granada, 18071 Granada, Spain.* <sup>e</sup> *Departamento de Química Inorgánica, Universidad de Granada, 18071, Granada, Spain.* <sup>f</sup> *Departamento de Química Aplicada, Facultad de Química, Universidad del País Vasco/Euskal Herriko Unibertsitatea, UPV/EHU, 20018, San Sebastián, Spain.*

### Contents:

- S1. SEM micrographs.
- S2. Selected bonds and angles of enantiomeric pairs of compounds **1-L** and **1-D**.
- S3. Thermogravimetric analyses under N<sub>2</sub> flow.
- S4. PXRD analysis of compounds **1-L** and **1-D**.
- S5. N<sub>2</sub> adsorption-desorption isotherms at 77 K.
- S6. Diffuse reflectance results.
- S7. Photoluminescence measurements.
- S8. Lifetime measurements.
- S9. TD-DFT computational details.
- S10. Circularly Polarized Luminescence measurements.
- S11. Statistical analysis of the CPL data.

## S1. SEM micrographs

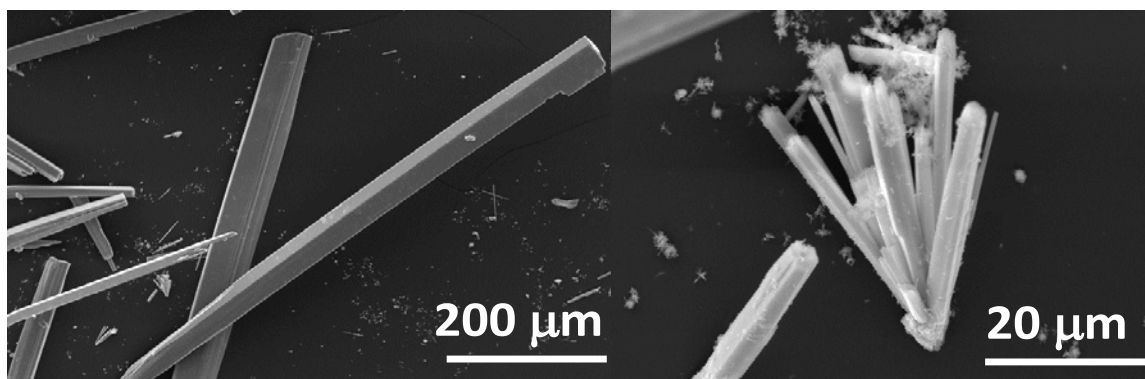


**Figure S1.** SEM micrographs on crystals of compound **1-L**.

## S2. Selected bonds and angles of enantiomeric pairs of compound 1

Table S1. Selected distances (Å) and angles (°) for compound 1-L.

Distances		Angles			
Ba1 O1A	2.757(6)	O1A Ba1 O1B	151.4(2)	O1D Ba2 O2A	94.9(2)
Ba1 O1B	2.829(6)	O1A Ba2 O1B	149.2(2)	O1D Ba2 O2B	71.7(2)
Ba1 O1C	2.766(6)	O1A Ba1 O1C	88.5(2)	O1D Ba2 O2B	87.6(2)
Ba1 O1D	3.026(6)	O1A Ba1 O1C	76.2(2)	O1D Ba2 O2C	148.9(2)
Ba1 O2C	2.984(6)	O1A Ba1 O1D	63.2(2)	O1D Ba2 O2D	44.9(2)
Ba1 O2D	2.715(6)	O1A Ba2 O1D	64.6(2)	O1D Ba1 O2D	78.5(2)
Ba1 O2D	2.764(6)	O1A Ba2 O2A	75.1(2)	O1D Ba1 O2D	126.5(3)
Ba1 O3A	2.794(8)	O1A Ba2 O2A	45.4(2)	O1D Ba2 O3C	128.4(6)
Ba2 O1A	2.905(6)	O1A Ba2 O2B	124.8(2)	O2A Ba2 O1B	108.4(2)
Ba2 O1B	2.975(6)	O1A Ba2 O2B	97.8(2)	O2A Ba2 O1D	94.9(2)
Ba2 O1D	2.781(6)	O1A Ba1 O2C	90.1(2)	O2A Ba2 O2A	114.2(2)
Ba2 O2A	2.856(6)	O1A Ba2 O2C	136.1(2)	O2A Ba2 O2B	64.4(2)
Ba2 O2A	2.777(6)	O1A Ba1 O2D	90.9(2)	O2A Ba2 O2C	124.8(2)
Ba2 O2B	2.919(5)	O1A Ba1 O2D	77.9(2)	O2B Ba2 O2B	112.5(2)
Ba2 O2B	2.768(5)	O1A Ba1 O3A	138.7(2)	O2B Ba2 O2C	98.4(2)
Ba2 O2C	2.772(6)	O1B Ba1 O1C	96.9(2)	O2C Ba1 O1D	152.1(2)
Ba2 O3B	2.855(8)	O1B Ba1 O1D	134.3(2)	O2C Ba2 O2A	93.1(2)
Ba2 O3C	3.03(3)	O1B Ba2 O2B	44.5(2)	O2C Ba2 O2B	68.7(2)
		O1B Ba2 O2B	71.4(2)	O2C Ba1 O2D	105.0(2)
		O1B Ba1 O2C	67.3(2)	O2D Ba1 O1A	90.9(2)
		O1B Ba2 O2C	68.1(2)	O2D Ba1 O2D	119.3(2)
		O1B Ba1 O2D	93.2(2)	O3A Ba1 O1B	69.6(2)
		O1B Ba1 O2D	123.5(2)	O3A Ba1 O1C	114.8(2)
		O1C Ba1 O1B	68.8(2)	O3A Ba1 O1D	81.4(2)
		O1C Ba1 O1C	114.4(2)	O3A Ba1 O2C	126.5(2)
		O1C Ba1 O1D	96.8(2)	O3A Ba1 O2D	76.8(2)
		O1C Ba1 O1D	127.7(2)	O3B Ba2 O1A	73.7(2)
		O1C Ba1 O2C	73.2(2)	O3B Ba2 O1B	136.9(2)
		O1C Ba1 O2C	44.2(2)	O3B Ba2 O1D	132.8(2)
		O1C Ba1 O2D	61.7(2)	O3B Ba2 O2A	68.6(2)
		O1C Ba1 O2D	166.4(2)	O3B Ba2 O2B	120.7(2)
		O1C Ba1 O2D	166.8(2)	O3B Ba2 O2C	77.9(2)
		O1C Ba1 O2D	61.1(2)	O3B Ba2 O3C	70.6(6)
		O1C Ba1 O3A	117.7(2)	O3C Ba2 O1A	135.7(6)
		O1D Ba2 O1A	64.6(2)	O3C Ba2 O1B	69.4(6)
		O1D Ba1 O1A	63.2(2)	O3C Ba2 O2A	68.7(6)
		O1D Ba2 O1B	85.8(2)	O3C Ba2 O2B	58.8(6)

**Table S2.** Selected distances (Å) and angles (°) for **1-D**.

Distances		Angles			
Ba1 O1A	2.757(6)	O1A Ba1 O1A	112.7(1)	O1D Ba2 O2D	44.9(1)
Ba1 O1B	2.829(6)	O1A Ba1 O2A	71.7(1)	O1D Ba2 O3B	74.6(1)
Ba1 O1C	2.766(6)	O1A Ba1 O2A	44.5(1)	O1C Ba2 O3C	61.3(1)
Ba1 O1D	3.026(6)	O1A Ba1 O3A	120.1(1)	O1D Ba2 O3C	62.2(1)
Ba1 O2C	2.984(6)	O1A Ba1 O3A	121.0(1)	O2A Ba1 O3A	137.2(1)
Ba1 O2D	2.715(6)	O1A Ba1 O1B	97.2(1)	O2A Ba1 O1B	149.0(1)
Ba1 O2D	2.764(6)	O1A Ba1 O1B	124.6(1)	O2A Ba2 O1B	150.9(1)
Ba1 O3A	2.794(8)	O1A Ba1 O2B	65.0(1)	O2A Ba1 O1C	68.1(1)
Ba2 O1A	2.905(6)	O1A Ba1 O2B	64.5(1)	O2A Ba1 O2B	108.6(1)
Ba2 O1B	2.975(6)	O1A Ba1 O2B	165.7(1)	O2A Ba1 O2B	136.7(1)
Ba2 O1D	2.781(6)	O1A Ba1 O2B	166.3(1)	O2A Ba1 O2C	70.1(3)
Ba2 O2A	2.856(6)	O1A Ba1 O1C	68.5(1)	O2A Ba1 O2D	85.5(1)
Ba2 O2A	2.777(6)	O1A Ba1 O1C	98.9(1)	O2A Ba2 O1C	67.3(1)
Ba2 O2B	2.919(5)	O1A Ba1 O2C	122.8(3)	O2A Ba2 O1D	123.7(1)
Ba2 O2B	2.768(5)	O1A Ba1 O2C	60.2(3)	O2A Ba2 O1D	92.7(1)
Ba2 O2C	2.772(6)	O1A Ba1 O2D	87.5(1)	O2A Ba2 O2D	133.9(1)
Ba2 O3B	2.855(8)	O1A Ba1 O2D	71.0(1)	O2A Ba2 O3B	70.2(1)
Ba2 O3C	3.03(3)	O1B Ba1 O2B	45.3(1)	O2A Ba2 O3C	68.2(1)
		O1B Ba1 O2B	75.2(1)	O2A Ba2 O3C	96.9(1)
		O1B Ba1 O2B	45.3(1)	O2B Ba1 O1C	125.3(1)
		O1B Ba1 O2C	135.5(3)	O2B Ba1 O2B	114.0(1)
		O1B Ba1 O2D	64.7(1)	O2B Ba1 O2C	133.1(3)
		O1B Ba2 O1C	89.8(1)	O2B Ba1 O2D	78.4(1)
		O1B Ba2 O1D	91.3(1)	O2C Ba1 O1C	58.5(3)
		O1B Ba2 O1D	78.1(1)	O2C Ba1 O2B	69.0(3)
		O1B Ba2 O2D	63.5(1)	O2C Ba1 O2D	129.2(3)
		O1B Ba2 O3B	138.5(1)	O2D Ba2 O3C	97.1(1)
		O1B Ba2 O3C	88.4(1)	O3A Ba1 O1B	73.6(1)
		O1B Ba2 O3C	76.1(1)	O3A Ba1 O2B	68.4(1)
		O1C Ba1 O1A	98.9(1)	O3A Ba1 O2B	69.9(1)
		O1C Ba1 O2A	68.1(1)	O3A Ba1 O2C	69.9(3)
		O1C Ba1 O3A	78.5(1)	O3A Ba1 O2D	132.7(1)
		O1C Ba1 O1B	135.9(1)	O3B Ba2 O1C	126.9(1)
		O1C Ba1 O2B	92.8(1)	O3B Ba2 O1D	76.4(1)
		O1C Ba1 O2B	125.3(1)	O3B Ba2 O2D	81.0(1)
		O1C Ba1 O2C	58.5(3)	O3B Ba2 O3C	115.3(1)
		O1C Ba1 O2D	148.4(1)	O3C Ba2 O1C	72.6(1)
		O1D Ba2 O1C	119.8(1)	O3C Ba2 O1D	166.9(1)
		O1D Ba2 O1D	104.6(1)	O3C Ba2 O1D	61.3(1)
		O1C Ba2 O1D	134.8(1)	O3C Ba2 O2A	96.9(1)
		O1C Ba2 O2A	67.3(1)	O3C Ba2 O2D	97.1(1)
		O1C Ba2 O2D	152.1(1)	O3C Ba2 O2D	128.3(1)
		O1D Ba2 O2D	44.9(1)	O3C Ba2 O3B	118.1(1)
		O1D Ba2 O2D	79.2(1)	O3C Ba2 O3C	113.3(1)

### S3. Thermogravimetric analyses under synthetic air flow

The analysis of the TG curve has been done for compound **1-L** as a reference for both compounds in order to confirm the chemical formula proposed because of the rest of characterization.

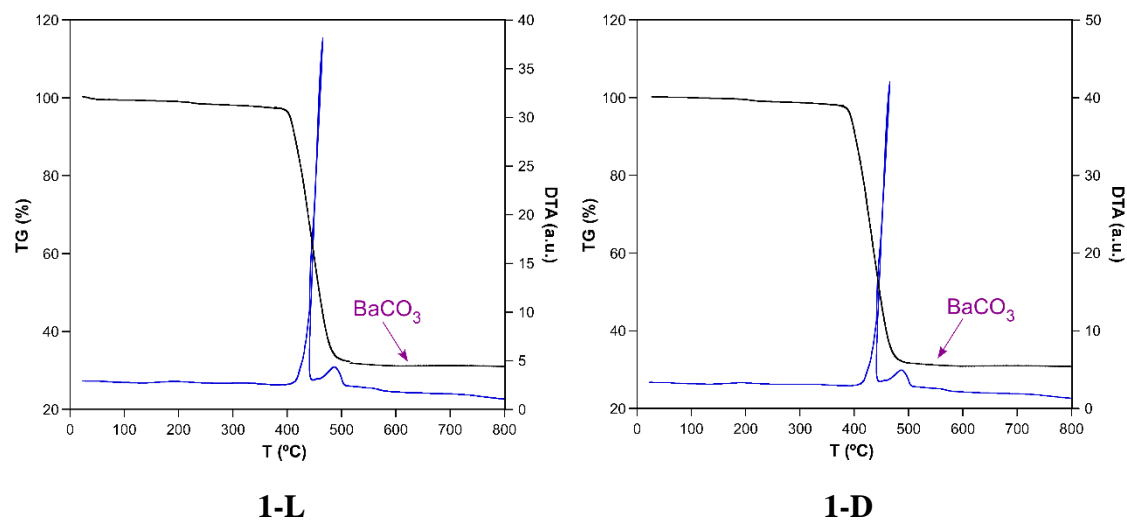


**Figure S2.** TGA and DTA curves of compounds **1-L** and **1-D**.

#### S4. Powder X-ray diffraction analysis of compounds 1-L and 1-D.

Experimentally measured powder X-ray diffraction data have been compared with those directly calculated from the single crystal X-ray data. Comparison of both diffractograms confirms the purity on both compounds.

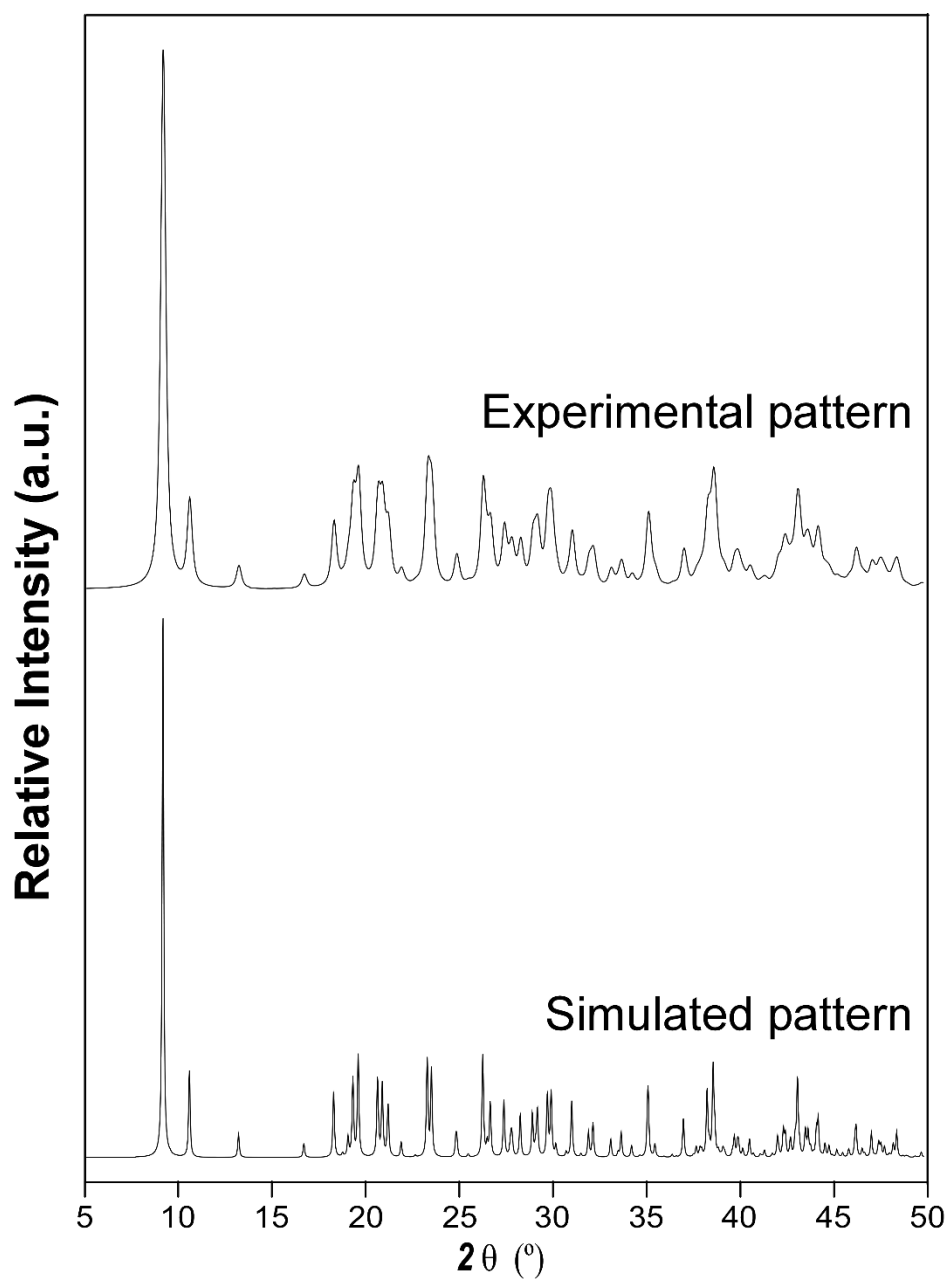


**Figure S3.** Experimental and simulated diffraction patterns for compound **1-L**.

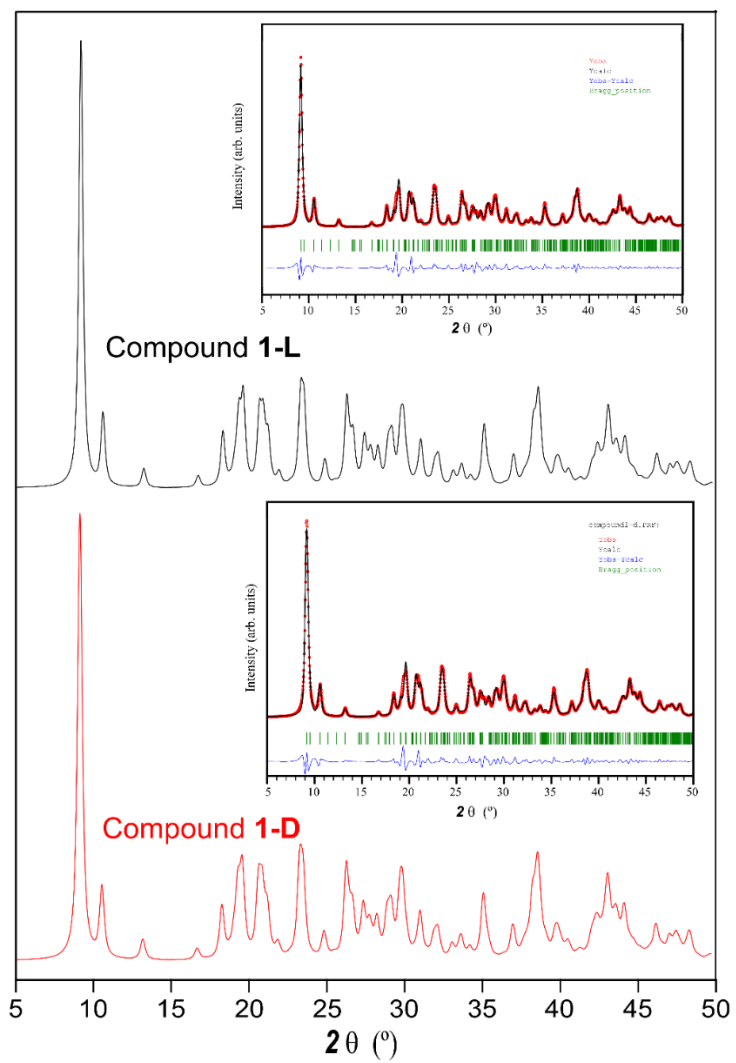


**Figure S4.** Comparison of the experimental PXRD for compounds **1-L** and **1-D**.

**S5. N<sub>2</sub> adsorption-desorption isotherms at 77 K**

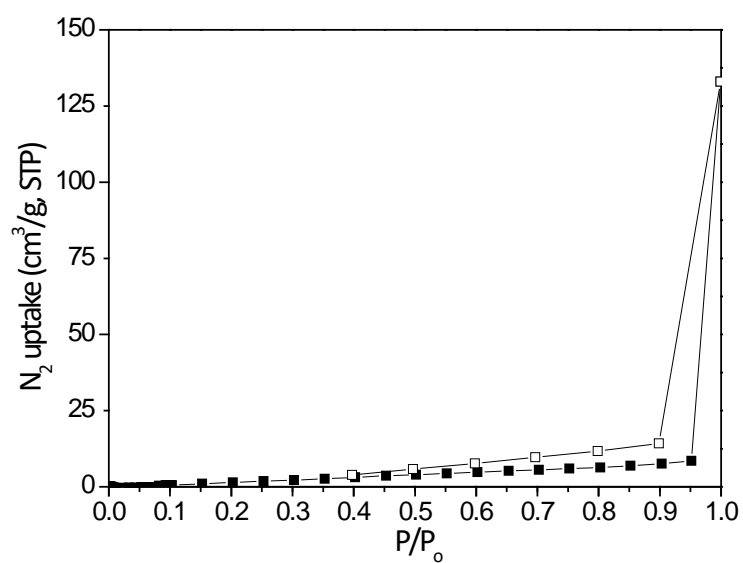


**Figure S5.** N<sub>2</sub> adsorption–desorption isotherms at 77 K for compound **1-L**.

## S6. Diffuse reflectance results.

The diffuse reflectance spectrum was measured for **1-L** as a representative compound and converted into a Tauc plot by applying the Kubelka-Munk function, which allows estimating the optical band gap of the compound.

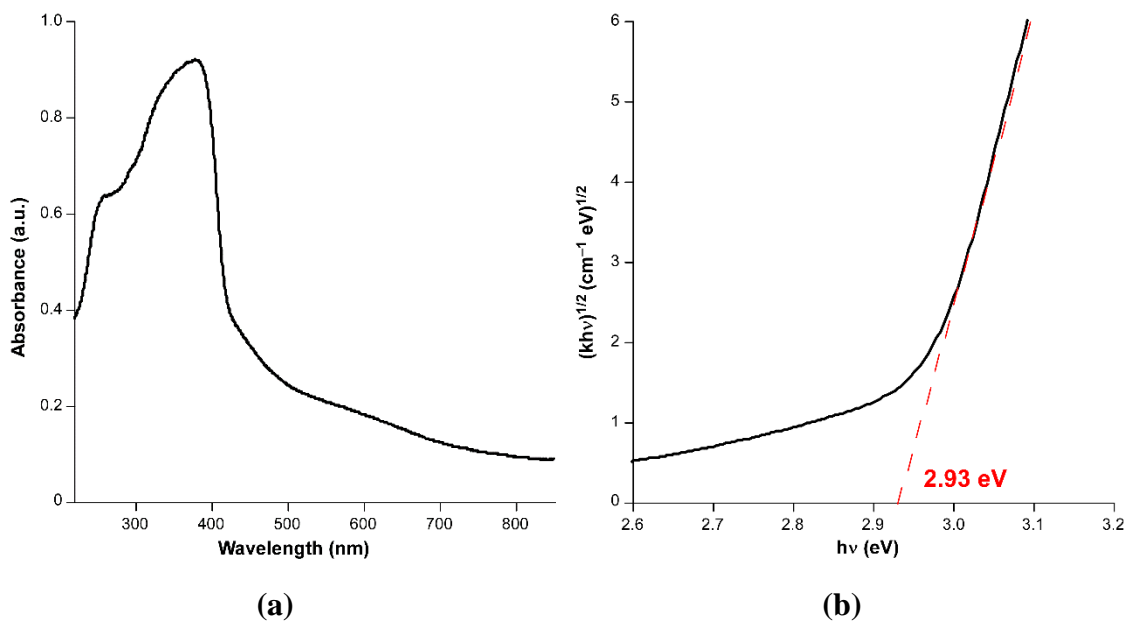


**Figure S6.** Diffuse reflectance data in the form of (a) absorption spectrum and (b) Tauc plot showing the estimated band gap for **1-L**.

## S7. Photoluminescence measurements.

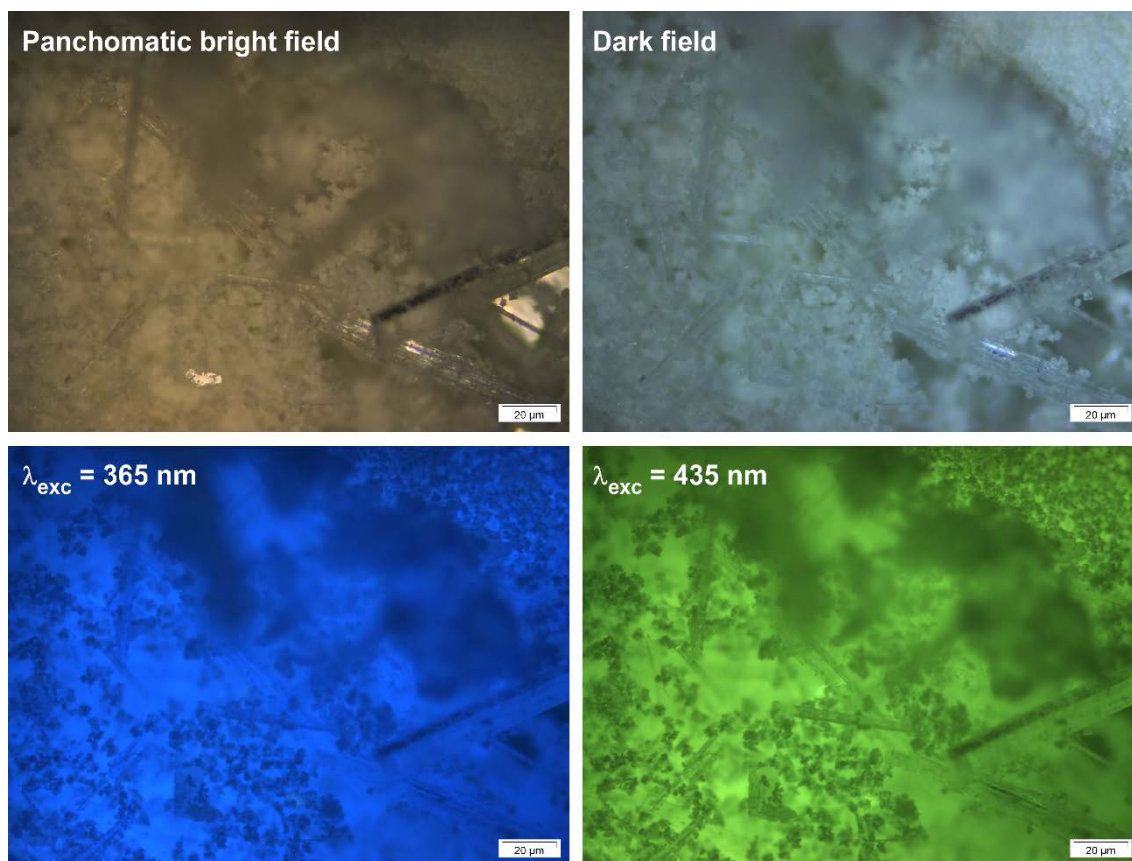


**Figure S7.** Emission micrographs for polycrystalline sample of compound **1-L**.

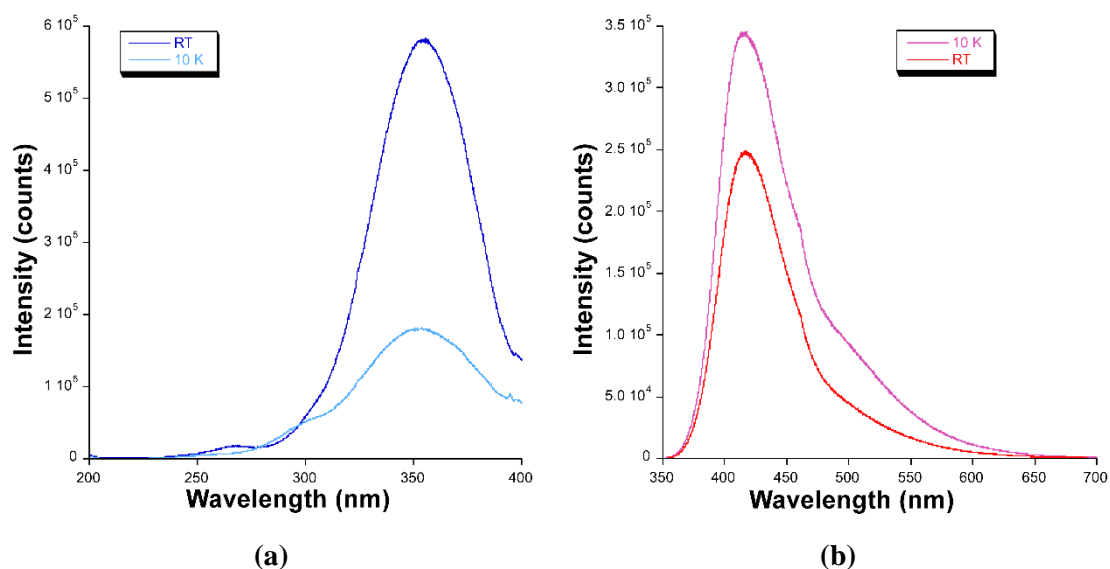


**Figure S8.** Comparison of (a) excitation and (b) emission spectra of compound **1-L** at room temperature and 10 K.

Additionally, the PL excitation and emission spectra have been measured for the ligands. Considering that the initial reagent employed in the synthesis mixture is glutamine, but it undergoes cyclization during the solvothermal procedure giving pyroglutamate, the polycrystalline samples of both compounds have been measured. This study was

accomplished only with L-specimens since no change is expected for the D-enantiomers. Note that the following spectra have been recorded using a different setup in the equipment necessary as to achieve an intense and reproducible emission profile, for which the counts measured in the intensity axis are not given.

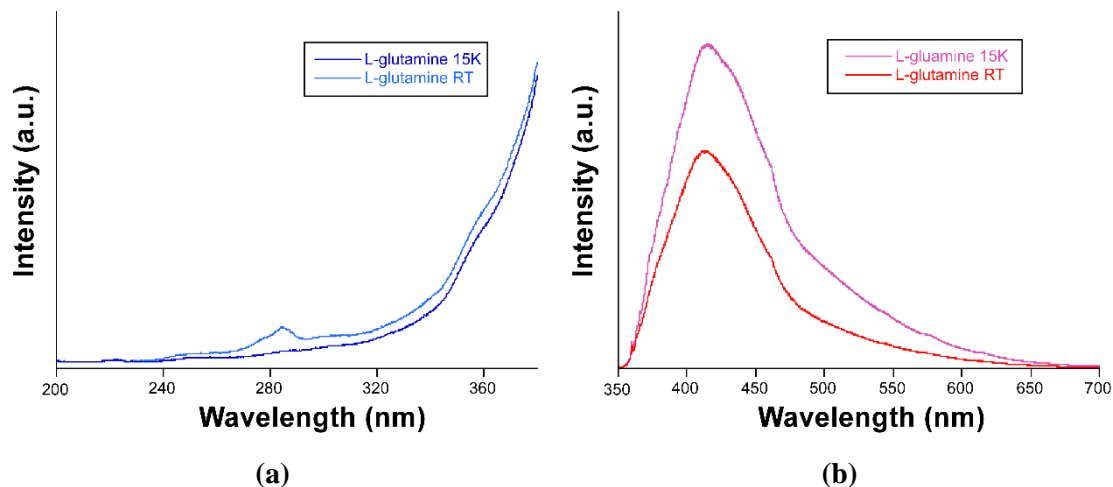


**Figure S9.** Comparison of (a) excitation ( $\lambda_{em} = 415$  nm) and (b) emission spectra ( $\lambda_{ex} = 325$  nm, He-Cd LASER) of the free L-glutamine ligand at room temperature and 10 K.

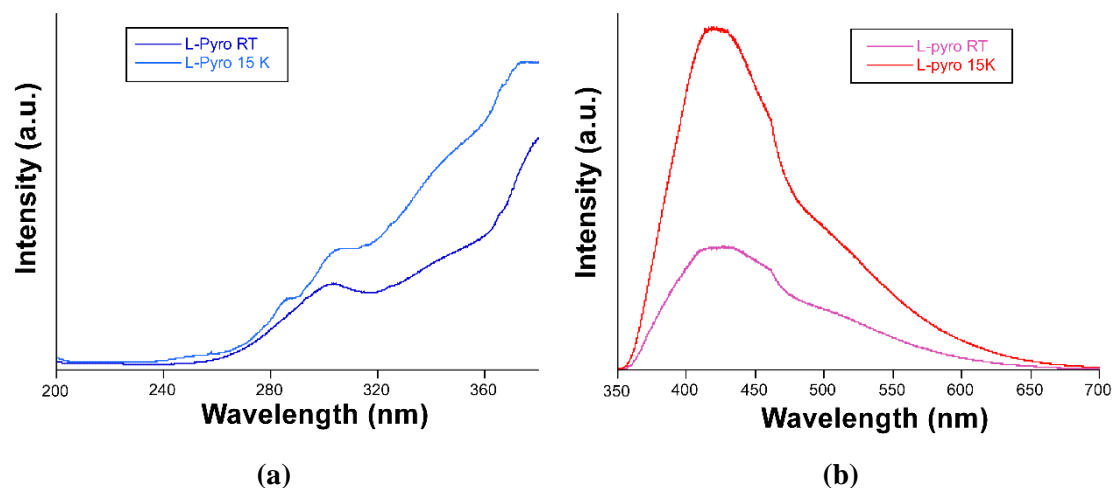


**Figure S10.** Comparison of (a) excitation ( $\lambda_{em} = 415$  nm) and (b) emission spectra ( $\lambda_{ex} = 325$  nm, He-Cd LASER) of the free L-pyroglutamate ligand at room temperature and 10 K.

As observed, there is no significant change in the shape of the emission band of the ligands, but for the fact that the band maximum of L-pyro is somewhat wider than that of L-glutamine. The main difference of with respect to the compounds PL is that the strong excitation maximum ( $\lambda = 354$  nm) observed for compounds **1-L** and **1-D** is much weaker for the free ligands.

The following figures show the emission colors of single crystals of both reagents in the images taken on a microscope possessing a Hg lamp and a camera coupled. From these images, it can be clearly observed that the different shape of these crystals compared to the needles formed in the case of compounds **1-L** and **1-D**.

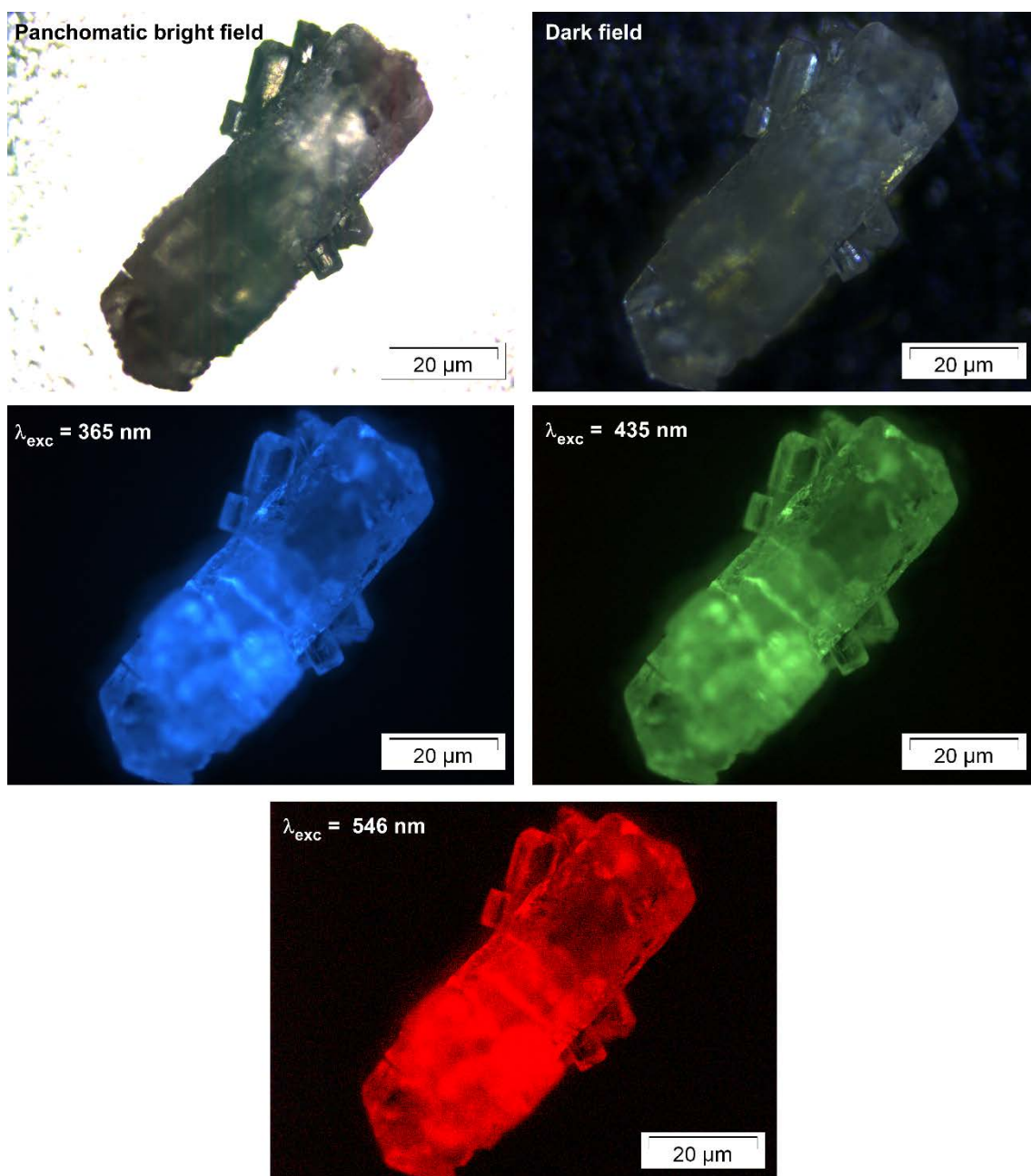


**Figure S11.** Micro-PL photographs taken on crystals of L-pryo sample. It is observed that the red emission is much weaker than blue and green given its poor definition.

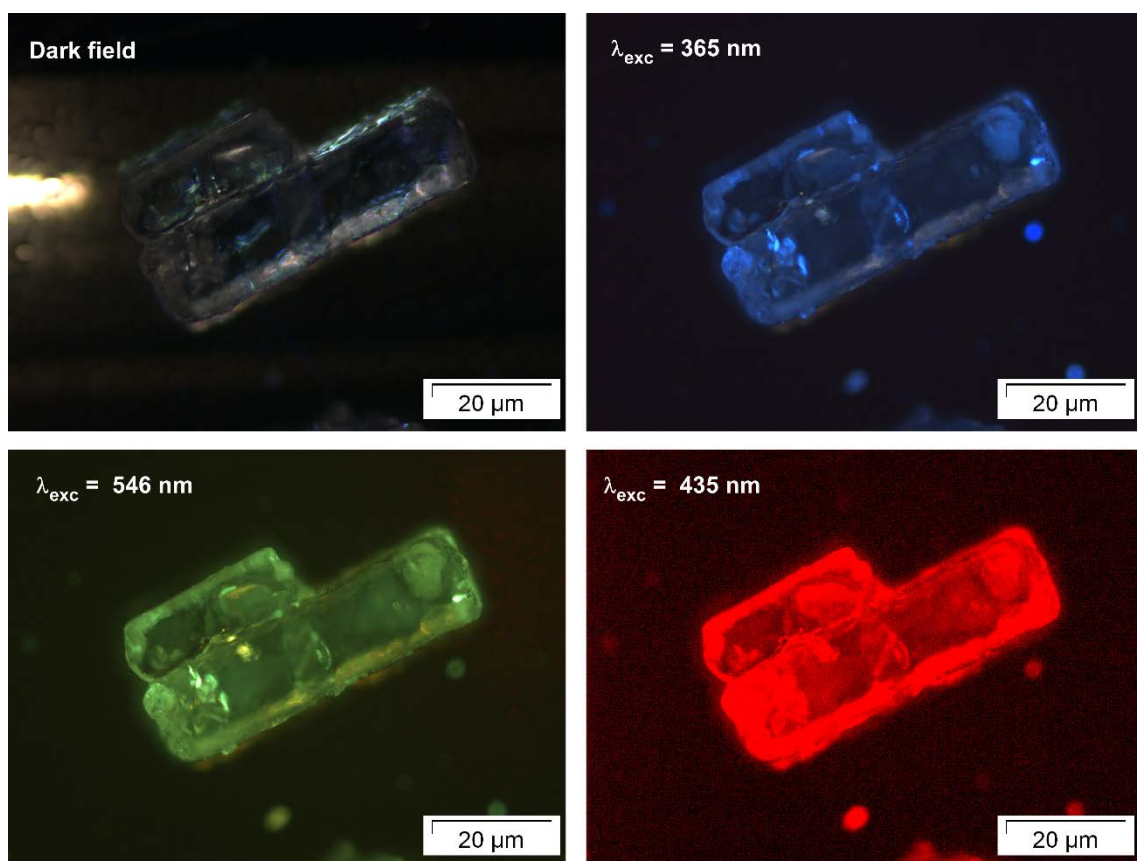


**Figure S12.** Micro-PL photographs taken on crystals of L-glutamine sample. It is observed that the red emission is much weaker than blue and green given its poor definition.

Finally, to corroborate the fact that the photoluminescence properties undoubtedly arise from the metal-organic material (compounds **1-L** and **1-D**), the spectra of the physical mixture of the components in the corresponding stoichiometry (barium(II) nitrate:pyroglutamate:formate in 2:2:1) has been also acquired. It must be noted that the resulting mixture does not possess the appropriate Ba:NO<sub>3</sub> stoichiometry because of the inherent 1:2 stoichiometry present in Ba(NO<sub>3</sub>)<sub>2</sub> salt. As observed, this mixture shows a very different emission spectrum compared to compounds **1-L** and **1-D**.

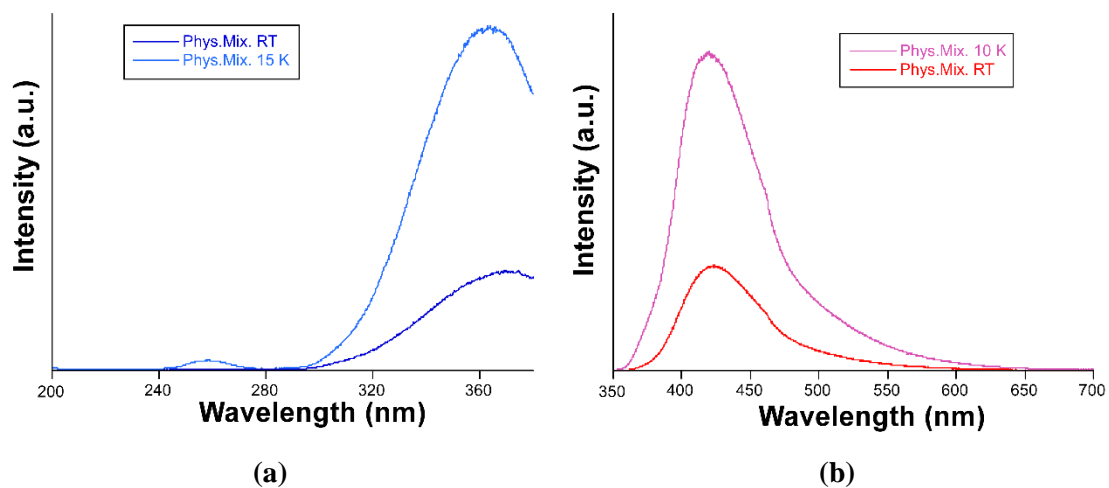


**Figure S13.** Photoluminescence properties of the physical mixture of the initial reagents in stoichiometric amounts: **(a)** excitation ( $\lambda_{em} = 420$  nm) and **(b)** emission spectra ( $\lambda_{ex} = 325$  nm, He-Cd LASER) spectra.

### S8. Lifetime measurements.

As shown in Table S3, the fitting of decay curves (see Figure S6) of compound **1-L** at RT reveals a uniform large lifetime of ca. 250 ms in the region of  $\lambda_{em} \approx 500$  nm, which explains the dim greenish afterglow observed just after the illumination under UV light. The curves related with the phosphorescent emission are well fitted with a bi-exponential expression [ $I_t = A_0 + A_1\exp(-t/\tau_1) + A_2\exp(-t/\tau_2)$ ] expression, which responds to the occurrence of two radiative processes.

**Table S3.** Lifetime values and corresponding percentages for components obtained from best fittings of decay curves measured at room temperature for compound **1-L** ( $\lambda_{ex} = 325$  nm).

Fluorescence			Phosphorescence			
$\lambda(\text{nm})$	$\tau_1$ ( $\mu\text{s}$ )	Chi Sq.	$\lambda(\text{nm})$	$\tau_1$ (ms)	$\tau_2$ (ms)	Chi Sq.
			475	63(2) / 47%	245(4) / 53%	1.266
400	15(1)	1.125	500	68(1) / 49%	253(4) / 51%	1.252
			525	59(1) / 45%	236(3) / 55%	1.275

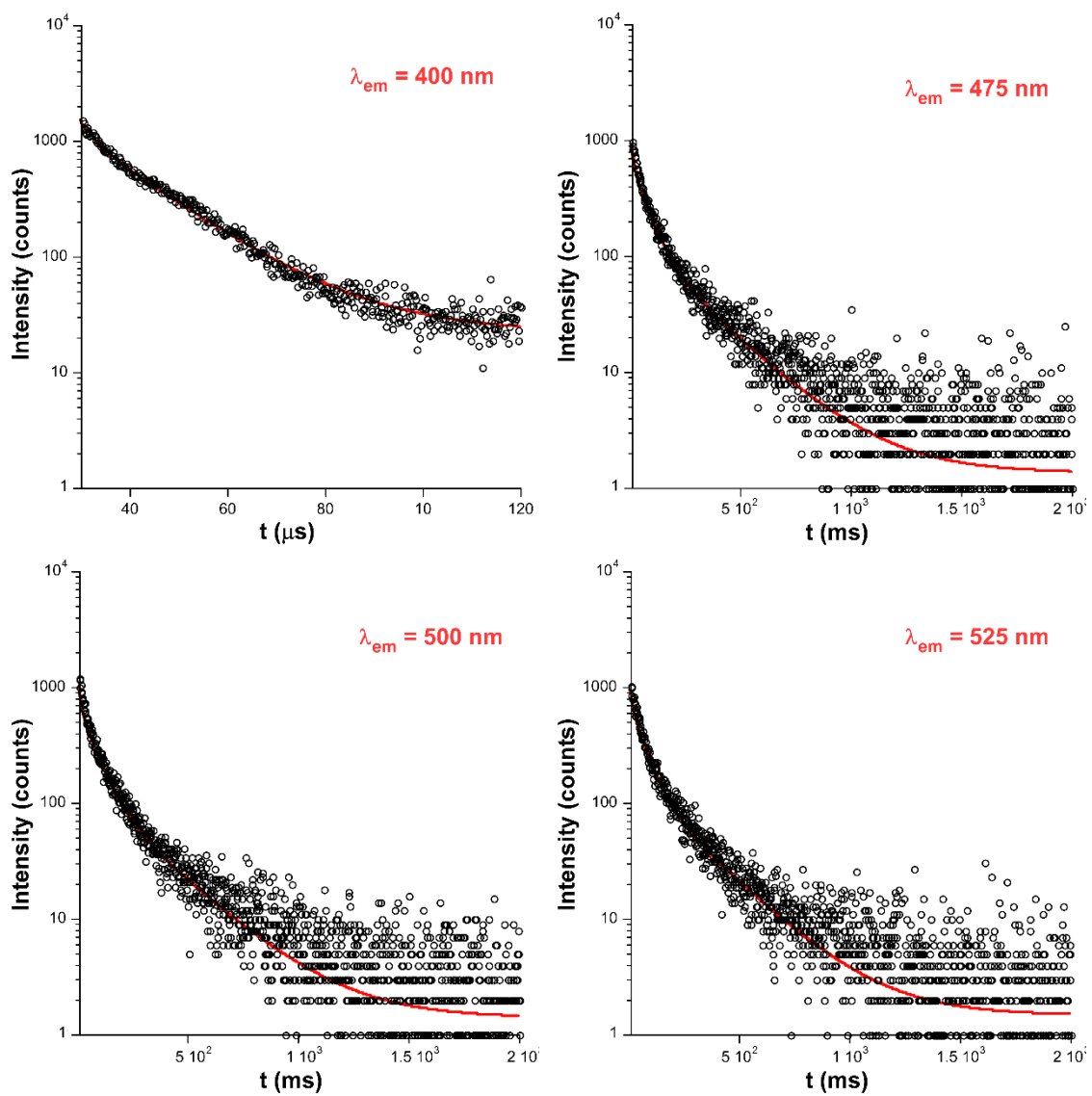
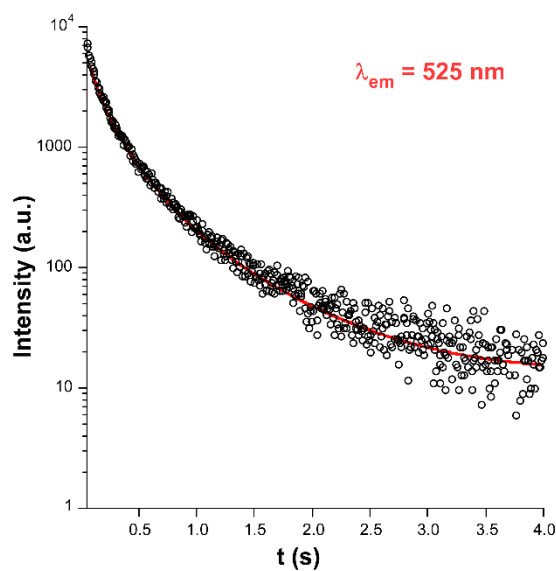
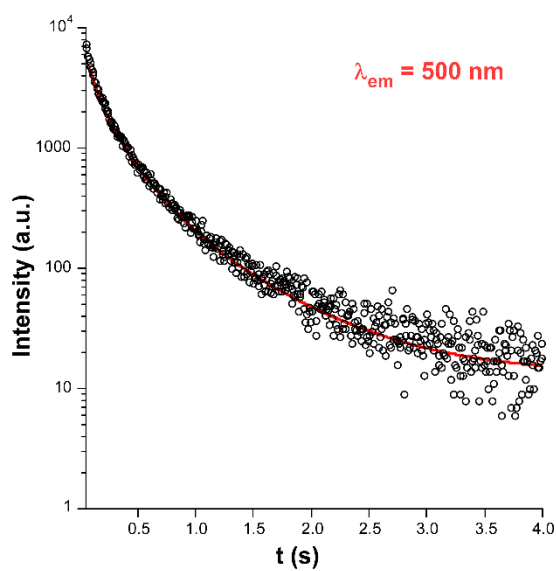
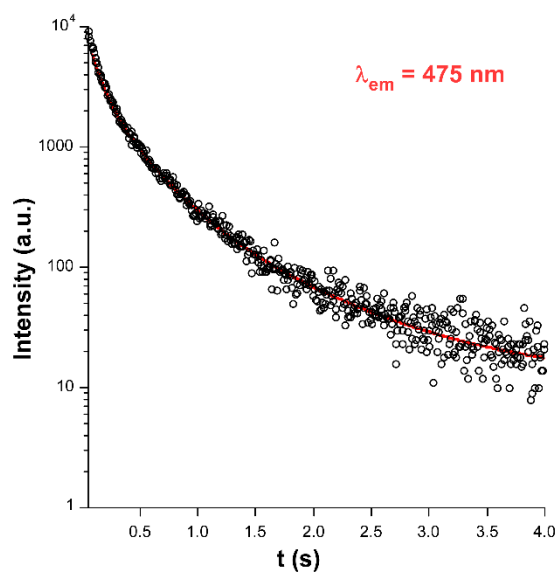
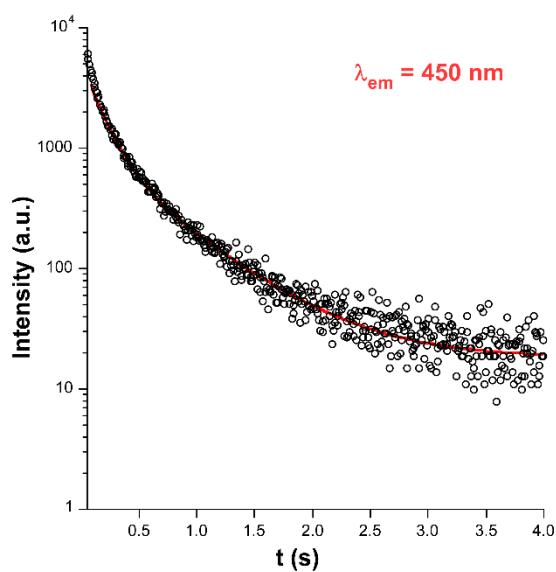
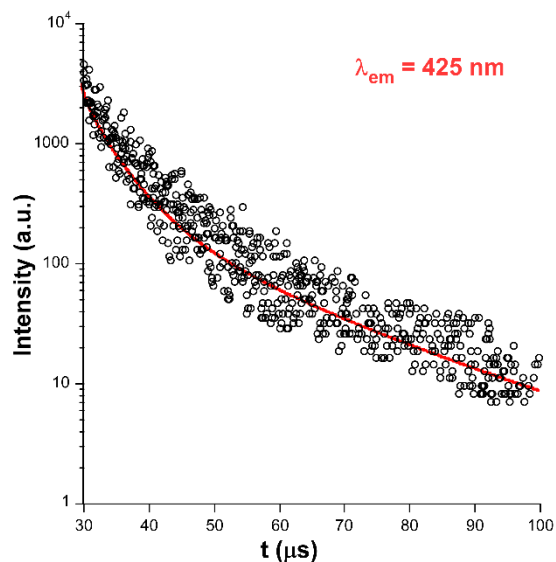
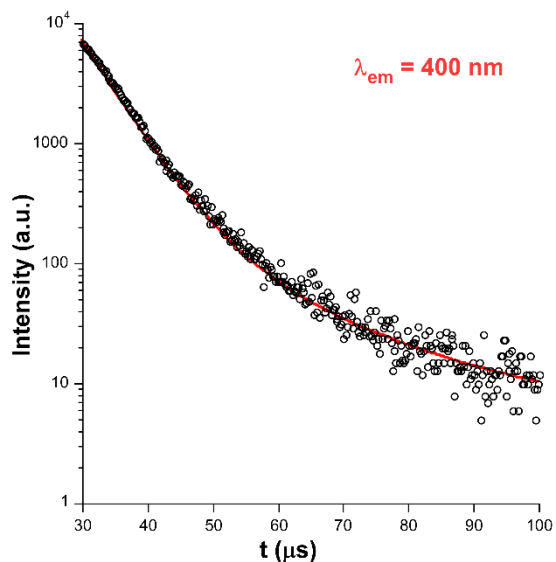
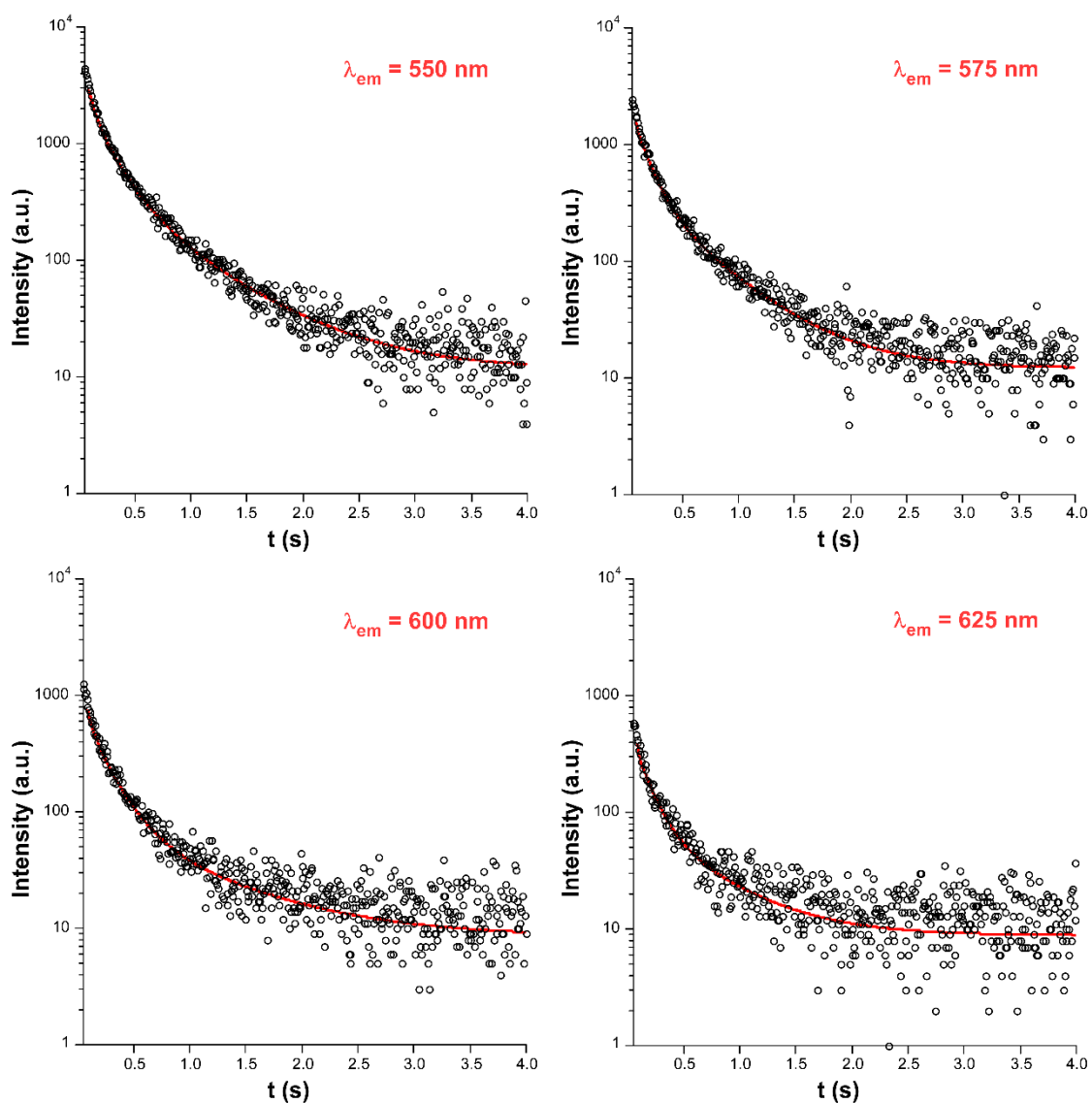


Figure S14. Room temperature decay curves for compound 1-L at selected emission wavelengths.

**Table S4.** Best fitting results from decay curves measured at 10 K for compound **1-L** ( $\lambda_{\text{ex}} = 325$  nm) at some selected emission wavelengths.

<b>Fluorescence</b>			
$\lambda$ (nm)	$\tau_1$ ( $\mu\text{s}$ )		Chi Sq.
400	17.0(5)		1.569
425	20.3(1)		1.539
<b>Phosphorescence</b>			
$\lambda$ (nm)	$\tau_1$ (ms)	$\tau_2$ (ms)	Chi Sq.
450	150(3) / 42%	585(8) / 57%	1.232
475	271(14) / 47%	787(36) / 37%	1.257
500	301(13) / 53%	872(93) / 29%	1.158
525	245(14) / 50%	700(33) / 35%	1.148
550	207(11) / 48%	663(25) / 41%	1.081
575	131(3) / 43%	521(11) / 56%	1.162
600	199(14) / 55%	449(78) / 38%	1.286
625	133(8) / 44%	456(33) / 55%	1.215





**Figure S15.** Decay curves for compound **1-L** at selected emission wavelengths recorded at 10 K.

For comparative purposes, the emission decay curves of the reagents have been also recorded both at room temperature and 15 K. From the fitting of the curves, it may be inferred that both samples characterize for a fluorescent emission composed of few nanoseconds, with no rest of long-lived signal observed in compounds **1-L** and **1-D**. The curves related with the fluorescent emission of L-glutamine ligand are well fitted with a mono-exponential expression [ $I_t = A_0 + A_1 \exp(-t/\tau_1)$ ] expression.

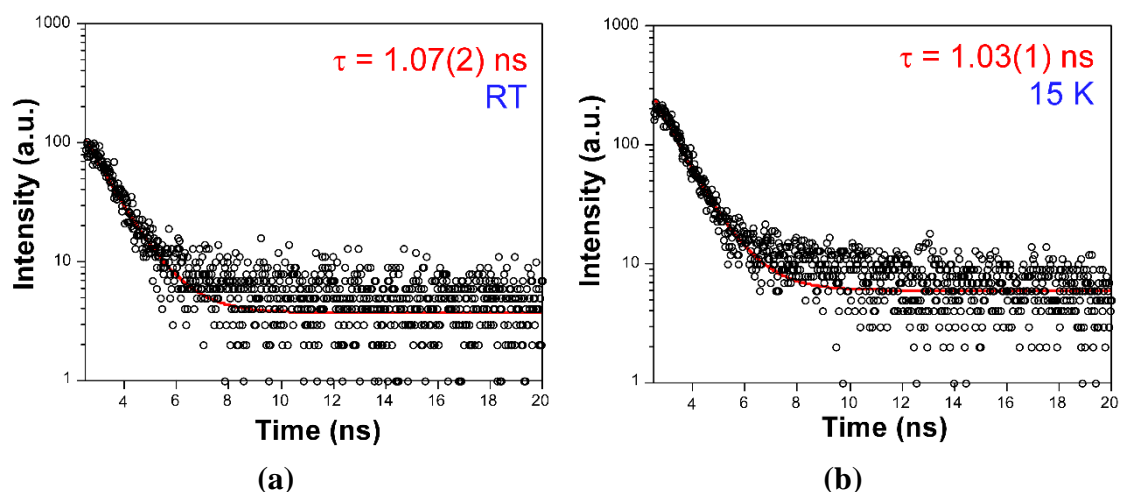


**Figure S16.** Decay curves acquired with  $\lambda_{\text{ex}} = 340$  nm and  $\lambda_{\text{em}} = 415$  nm for the L-glutamine ligand showing the best fit: (a) at room temperature and (b) at 15 K.

The short lifetime found for the pyro ligand requires the deconvolution of the decay curve as to give a quantitative result. To that end, the emission of the pulse (without sample) was used as the instrument reference, which shows a very short lifetime of ca. 0.3 ns corresponding to the pulse of the laser diode. The second (longer) lifetime represents the emission of the ligand.

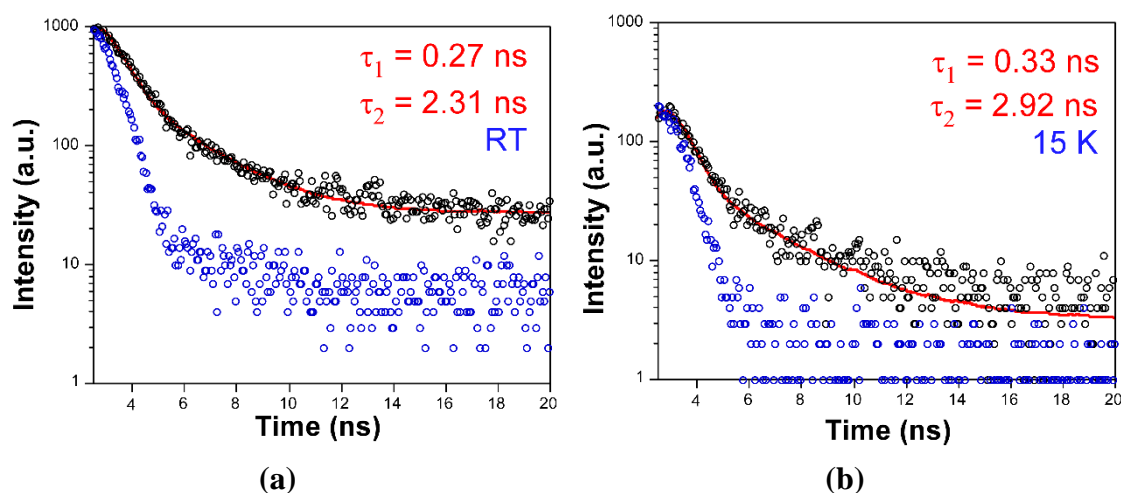


**Figure S17.** Decay curves acquired with  $\lambda_{\text{ex}} = 340$  nm and  $\lambda_{\text{em}} = 415$  nm for the L-pyro ligand showing the best fit: (a) at room temperature and (b) at 15 K.

Additionally, in the following figure is shown the decay curve of the emission of the physical mixture of the reagents of compound **1-L** in the corresponding stoichiometry. As observed, this mixture does not present the long-lived phosphorescent emission characteristic of the crystallized compounds. Instead, the emission lifetime is in the range of that shown by the compound the emission band maxima (of some microseconds, see first inset in Figure S14 and Table S4) and it does not hardly change with the temperature.

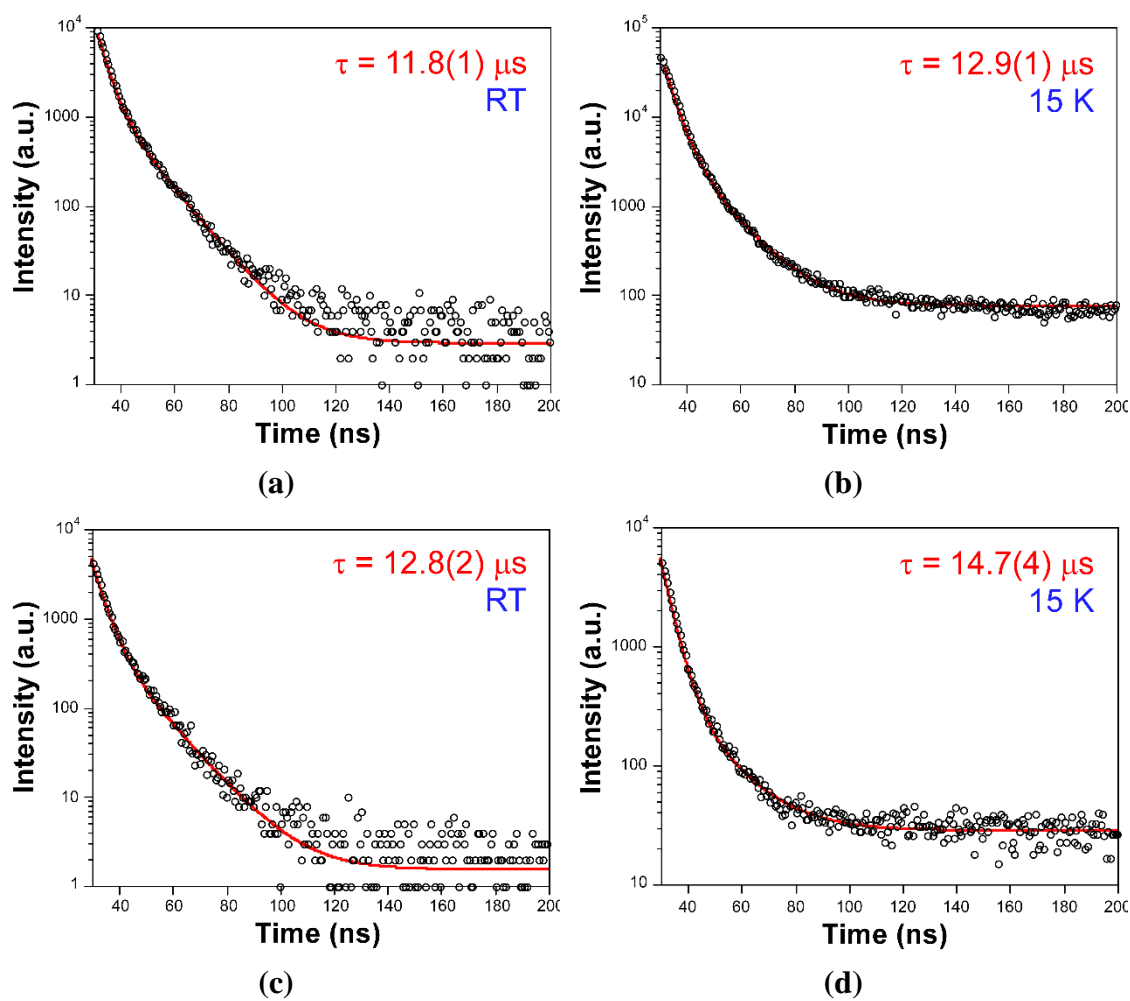
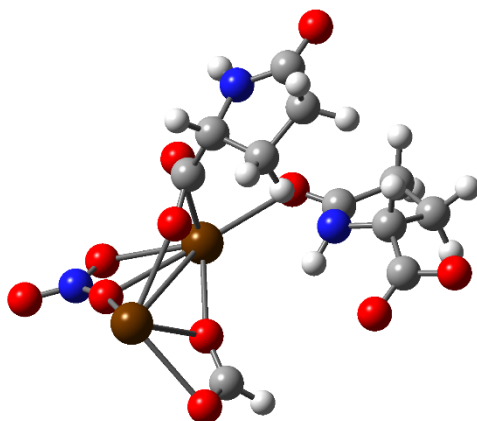


**Figure S18.** Decay curves of the physical mixture of the initial reagents in stoichiometric amounts with  $\lambda_{\text{ex}} = 340 \text{ nm}$ : (a)  $\lambda_{\text{em}} = 422 \text{ nm}$  at RT, (b)  $\lambda_{\text{em}} = 422 \text{ nm}$  at 15 K, (c)  $\lambda_{\text{em}} = 475 \text{ nm}$  at RT, (d)  $\lambda_{\text{em}} = 475 \text{ nm}$  at 15 K.

## S9. TD-DFT computational details.



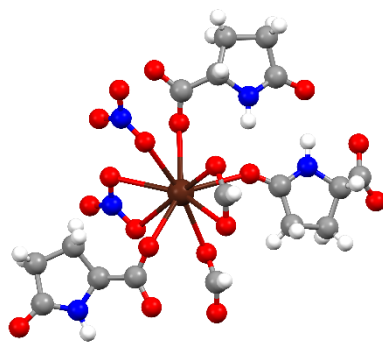
**Model 1**

**Figure S19.** Molecular representation of models of compounds **1-L** employed for the calculations.

**Table S5.** Calculated main excitation and emission energies (nm), singlet electronic transitions and associated oscillator strengths of model 1 in gas phase.

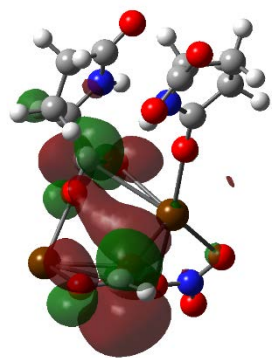
Exp. $\lambda$ (nm)	Calcd. $\lambda$ (nm)	Significant contributions	Osc. strength (a.u.)
Excitation energies			
267	260	HOMO – 6 $\rightarrow$ LUMO + 1 (99%)	0.115
354	350	HOMO $\rightarrow$ LUMO + 3 (99%)	0.179
Emission energies			
415	418	HOMO $\leftarrow$ LUMO (86%)	0.192

It must be added that a second model was also tested for carrying TD-DFT calculations, consisting of a bigger excerpt of the crystal structure in which the coordination shell was completed (named model 2), but it was not possible to converge the calculations even when the basis was significantly reduced.

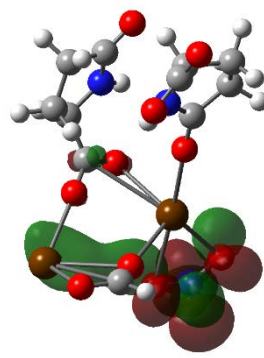


**Model 2**

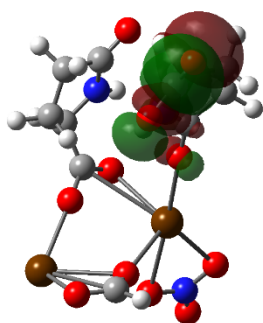
**Figure S20.** Molecular representation of models of compounds **1-L** employed for the calculations.



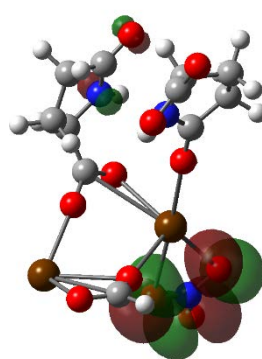
LUMO + 3



LUMO + 1

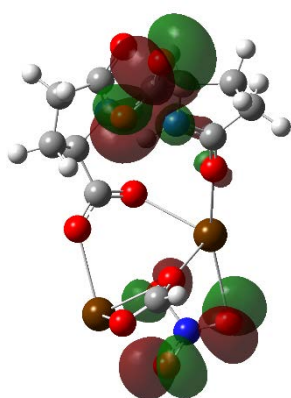


HOMO

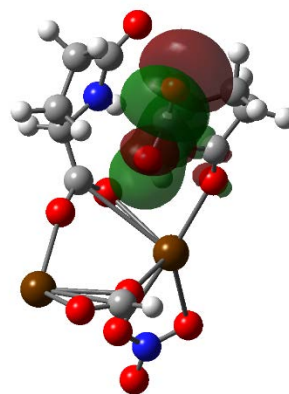


HOMO - 6

**Figure S21.** Highest Occupied and Lowest Unoccupied Molecular Orbitals of model 1 involved in the main singlet excitation charge transitions.



LUMO



HOMO

**Figure S22.** Highest Occupied and Lowest Unoccupied Molecular Orbitals of model 1 involved in the main singlet emission charge transitions.

### S10. Calculation of the lowest-lying triplet state ( $T_1$ ).

The  $T_1-S_0$  energy difference, which corresponds to the main phosphorescent emission line, has been estimated from vertical excitation performed for the optimized geometry of the lowest lying excited triplet state ( $T_1$ ). The triplet state geometry optimisation and frequencies calculation was performed on models 1 and 2 (Figure S31) with Gaussian 09 package, using the Becke three parameter hybrid functional with the non-local correlation functional of Lee-Yang-Parr (B3LYP) with the 6-311G++(d,p) basis set for all atoms. A fact about these MOs calculated at triplet state geometry that must be emphasized is that they show a similar shape regarding their singlet counterparts, with a  $\pi$  and  $\pi^*$  character respectively for HOMO and LUMO.

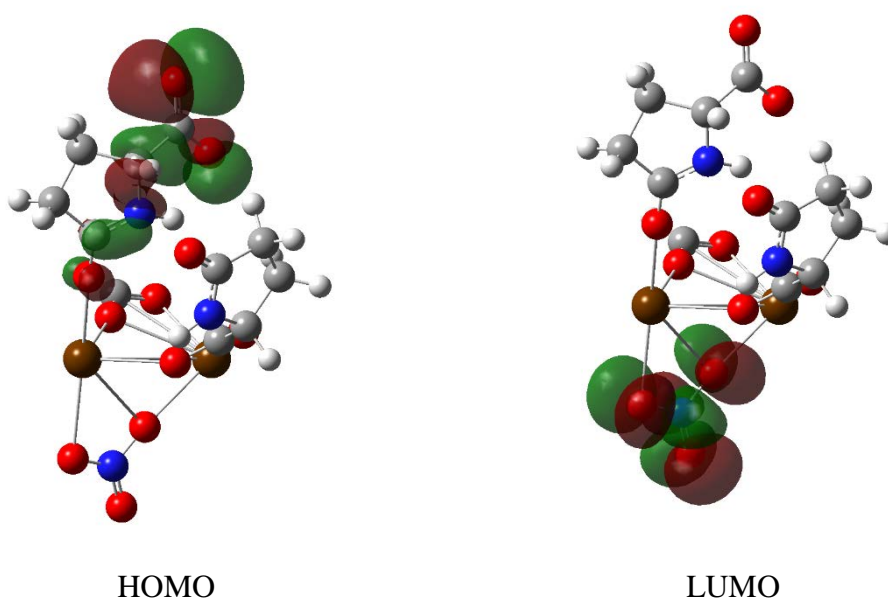


**Figure S23.** Highest Occupied and Lowest Unoccupied (single-occupied alpha) Molecular Orbitals converged at first excited triplet state geometry for model 1.

### S10. Circularly Polarized Luminescence measurements.

Emission and CPL measurements were performed in an Olis DSM172 spectrophotometer, using a fixed wavelength LED (250 nm) as the excitation source.

To prepare both samples for CPL measurements, 2 mg of **1-L** or **1-D** were ground into a finely divided powder. Then, they were mixed with 5-6 drops of mineral oil (Nujol) and the resulting homogeneous mixture was placed between 2 commercial potassium bromide tablets. This system was used directly for CPL measurements placed at a 45° angle relative to the excitation source. Other orientations were also checked yielding the same signal, thus ruling out the presence of any artefact derived from macro- or microanisotropies.<sup>1</sup> The resulting CPL spectra ( $g_{lum}$  and  $\Delta I$ ) are an average spectra obtained after 180 scans. Circularly polarization was confirmed by looking at the signal at a frequency of  $2 \times$  the frequency of the PEM acting as an oscillating quarter-wave plate.<sup>2</sup> The  $g_{lum}$  values were calculated following the expression:

$$g_{lum} = \frac{\Delta I}{\frac{1}{2}I} = \frac{I^L - I^R}{\frac{1}{2}(I^L + I^R)} \quad (\text{Eq. 1})$$

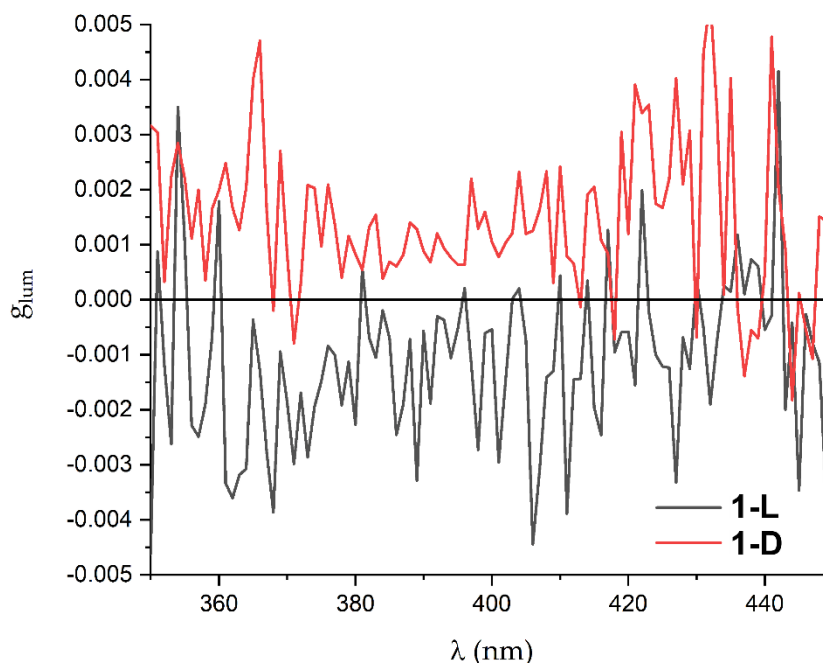


**Figure S24.**  $g_{lum}$  values of the CPL bands found for the main emission band of compounds **1-L** and **1-D**.

<sup>1</sup> E. Castiglioni, P. Biscarini and S. Abbate, *Chirality*, 2009, **21**, E28-E36.

<sup>2</sup>.- (a) H. P. J. M. Dekkers, P. F. Moraal, J. M. Timper and J. P. Riehl, *Appl. Spectrosc.*, 1985, **39**, 818. (b) J. P. Riehl and F. S. Richardson, *Chem. Rev.*, 1986, **86**, 1.

### S11. Statistical analysis of the CPL data.

Non-normalized  $\Delta I$  (i. e.  $I_L - I_R$ ) from **1-L** and **1-D** and the racemic mixture were used for the statistical analysis of the CPL activity, considering an approach based on the areas of the different spectra. Owing to the compounds are prepared in a enantiopure form and a 1:1 mixture of solid could result during the milling process in inhomogeneous material and therefore spurious chiroptical signals, we have created the racemic data using the mean of both set of data.

A set of 130 scans recorded for each enantiomer were divided into 13 groups of 10 scans and the corresponding average areas were calculated. In the case of the racemic data, the groups were prepared using the mean of the enantiomer data. Such racemic sets were randomized to avoid any relationship between the compared set of data. With those area values, a mean area and its standard deviation was calculated for the spectra of each compound. The data are shown in Figure S17 and TableS6.

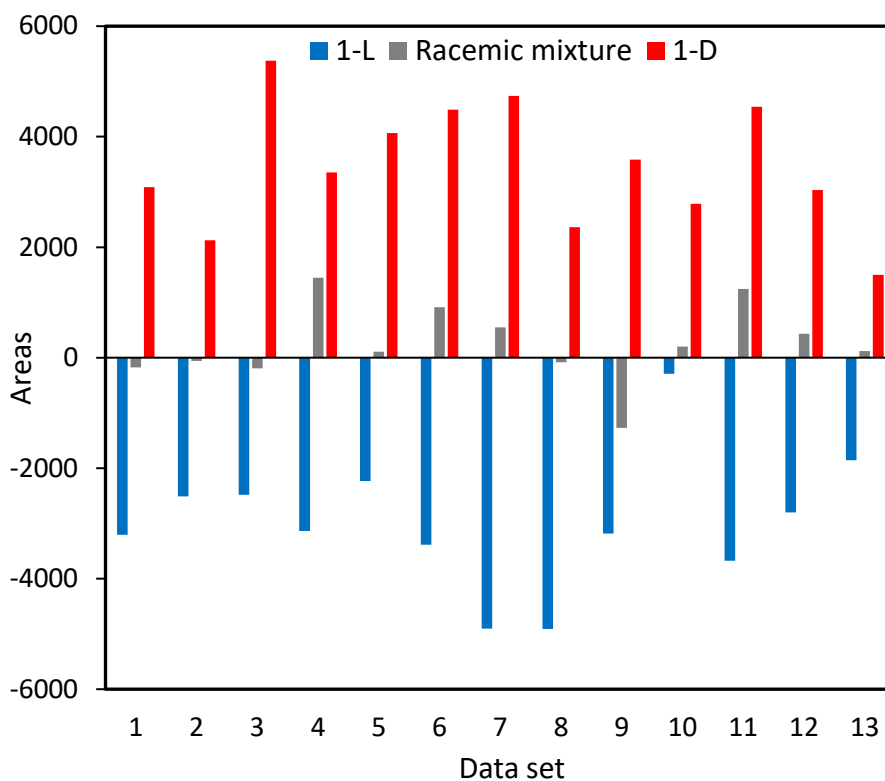


**Figure S25.** Areas of the different data set obtained from the CPL activity of compounds **1-L** (blue bars), **1-D** (red bars), and the racemic mixture (grey bars).

As the CPL signals can be positive or negative, negative values indicate that the spectra delimits a net area in the negative part of the scale. Notice that, while opposite signed areas were estimated for the racemic mixture, only positive areas resulted from the data treatment of **1-D** and only negative areas resulted from the data treatment of **1-L**.

**Table S6.** Statistic parameters for the areas obtained from CPL spectra.

Data set	Areas		
	1-D	1-L	Racemic mixture (RM)
1	3087.939126	-3206.62936	-177.3986158
2	2122.377647	-2513.072785	-59.34511714
3	5375.629922	-2481.127431	-195.3475687
4	3352.063107	-3137.187166	1447.251245
5	4064.692198	-2234.101703	107.4379708
6	4487.462357	-3386.45554	915.2952471
7	4736.533807	-4905.342996	550.5034085
8	2363.604569	-4910.467039	-84.40459405
9	3585.875152	-3182.996579	-1273.431235
10	2785.77375	-293.9438859	201.4392863
11	4539.706897	-3676.578309	1245.914932
12	3035.568706	-2798.509419	431.5642938
13	1499.136456	-1853.933688	118.5296437
<b>Average area (<math>\square</math>)</b>	3464.335669	-2967.718915	248.3083767
<b>Standard deviation (s)</b>	1137.357326	1215.816337	703.5884023
<b>Variance (s<sup>2</sup>)</b>	1293581.686	1478209.366	495036.6399

- **F-test**

$$F = \frac{s_1^2}{s_2^2} \quad (s_1 > s_2)$$

$H_0 \equiv s_1^2 = s_2^2$  ( $F_{\text{calc}} < F_{\text{tab}}$ ) Variances are not significantly different

$H_1 \equiv s_1^2 \neq s_2^2$  ( $F_{\text{calc}} \geq F_{\text{tab}}$ ) Variances are significantly different

**Table S7.** F-test for the area data (\*)

	$F_{\text{calc}}$	Conclusion
1-D	2.613	$F_{\text{calc}} > F_{\text{tab}} \rightarrow H_0$
1-L	2.986	$F_{\text{calc}} > F_{\text{tab}} \rightarrow H_0$

(\*) $F_{\text{tab}}$ , ( $\alpha = 0.05$ ;  $n_1=13$ ,  $n_2= 13$ ) = 2.147

Therefore, in all cases is concluded that the variances significantly differ.

- **t-test**

Additionally, aiming at the determination of the veracity of the acquired CPL signals for the **1-D** and **1-L** enantiomers, a t student statistical analysis was performed. To this end, a comparison with the data obtained for the racemic mixture was considered.

$$t = \frac{|\bar{x}_1 - \bar{x}_2|}{s_p \sqrt{\frac{1}{n_1} + \frac{1}{n_2}}}$$

$$s_p = \sqrt{\frac{(n_1 - 1)s_1^2 + (n_2 - 1)s_2^2}{n_1 + n_2 - 2}}$$

$H_0 \equiv s_1$  (enantiomer)  $\leq s_2$  (RM) ( $t_{\text{calc}} < t_{\text{tab}}$ ) Means are not significantly different  
 $H_1 \equiv s_1$  (enantiomer)  $> s_2$  (RM) ( $t_{\text{calc}} \geq t_{\text{tab}}$ ) Means are significantly different with the enantiomers giving a higher signal than the racemic mixture

**Table S8.** t-test for the area data of the CPL activity of the enantiomers vs. the racemic mixture (\*)

	$t_{\text{calc}}$	<b>Conclusion</b>
<b>1-D</b>	8.670	$t_{\text{calc}} > t_{\text{tab}} \rightarrow H_1$
<b>1-L</b>	8.255	$t_{\text{calc}} > t_{\text{tab}} \rightarrow H_1$

(\*)  $t_{\text{tab}}$  (one-tailed, 0.05;  $n_1=13$   $n_2=13$ ;  $df=24$ ) = 2.064;

Therefore, the results in **Table S7** suggest that, at 95% confidence, the signals observed for both enantiomers are significantly higher from the signals of the racemic mixture.